Turner's syndrome has shown that sensorineural hearing loss was negatively correlated with the serum concentration of IGF-1 (15), which suggests that hearing loss may be associated with the use of IGF-1R inhibitors.

In the PK analysis, no apparent drug–drug interaction between ganitumab and gemcitabine was observed. Similar AUC values of ganitumab between our study and a Japanese Phase 1 study in patients with advanced solid tumors (9) indicated that exposure to ganitumab 20 mg/kg would not be affected by the administration of gemcitabine. The mean C_{max} and AUC of gemcitabine in our study did not show any meaningful change between before and after administration of ganitumab. Gemcitabine is a small-molecule drug that is mainly eliminated by cytidine deaminase, whereas ganitumab is an immunoglobulin G1 monoclonal antibody considered to be mainly eliminated via catabolism. Therefore, a mechanism-based drug–drug interaction is not expected. The results on PK parameters in our study supported this expectation.

According to the exposure–response analysis, increased exposure to ganitumab was associated with prolonged progression-free survival and overall survival in patients with mPC (11). Since the ganitumab exposure at 20 mg/kg in our study appeared to be increased in a dose-dependent manner, when compared with that at 12 mg/kg in the Phase 2 study (10), further evaluation on the efficacy outcome at a ganitumab 20 mg/kg dose in patients with mPC is warranted.

No anti-ganitumab binding antibodies were detected in our study. In the previous single-agent study, anti-ganitumab binding antibodies were detected in one patient at Week 9, but no neutralizing antibodies were detected (8). In addition, the AUC values of ganitumab in this patient were similar after the first and third doses. Thus, we consider that the anti-ganitumab binding antibodies had no apparent effect on serum ganitumab concentrations.

Although assessment of efficacy was not a primary objective of our study, the combination of ganitumab and gemcitabine showed potential activity. Four patients (80%) achieved a best response of stable disease, and three (60%) had a time to progression longer than 100 days.

In conclusion, ganitumab 20 mg/kg combined with gemcitabine 1000 mg/m^2 was tolerable and showed an acceptable safety profile in Japanese patients with untreated mPC. Exposure to ganitumab at 20 mg/kg in our study was higher than that at 12 mg/kg in the previous Phase 2 study. Appropriateness of using the dose level of ganitumab 20 mg/kg for patients with mPC was confirmed by these findings, and the efficacy and safety of ganitumab 20 mg/kg combined with gemcitabine 1000 mg/m^2 were evaluated in the randomized Phase 3 study (GAMMA [Gemcitabine and AMG 479 in Metastatic Adenocarcinoma of the Pancreas], Clinical Trials gov. NCT01231347). However, this Phase 3 study was stopped because of futility. Currently, the other clinical data on efficacy, safety and PK are under analysis.

Acknowledgements

We thank the study coordinators, nurses and patients involved in the study; and Kenichi Hayashi (Alamedic Co., Ltd., Tokyo, Japan) for writing assistance.

Funding

This work was supported by Takeda Bio Development Center Limited (Tokyo, Japan). T.O. and A.F. received research funding from TBDC.

Conflict of interest statement

Y.K., K.S. and T.T. are employees of Takeda Bio Development Center Ltd. J.G. is employed in a leadership position and owns stock of Amgen Inc. M.I. has no conflict of interest to disclose.

References

1. Weroha SJ, Haluska P. IGF-1 receptor inhibitors in clinical trials—early lessons. *J Mammary Gland Biol Neoplasia* 2008;13:471–83.
2. Werner H, LeRoith D. The role of the insulin-like growth factor system in human cancer. *Adv Cancer Res* 1996;68:183–223.
3. Sachdev D, Yee D. Disrupting insulin-like growth factor signaling as a potential cancer therapy. *Mol Cancer Ther* 2007;6:1–12.
4. Macaulay VM. Insulin-like growth factors and cancer. *Br J Cancer* 1992;65:311–20.
5. Werner H, Le Roith D. New concepts in regulation and function of the insulin-like growth factors: implications for understanding normal growth and neoplasia. *Cell Mol Life Sci* 2000;57:932–42.
6. Ryan PD, Goss PE. The emerging role of the insulin-like growth factor pathway as a therapeutic target in cancer. *Oncologist* 2008;13:16–24.
7. Beltran PJ, Mitchell P, Chung YA, et al. AMG 479, a fully human anti-insulin-like growth factor receptor type I monoclonal antibody, inhibits the growth and survival of pancreatic carcinoma cells. *Mol Cancer Ther* 2009;8:1095–105.
8. Tolcher AW, Sarantopoulos J, Patnaik A, et al. Phase I, pharmacokinetic, and pharmacodynamic study of AMG 479, a fully human monoclonal antibody to insulin-like growth factor receptor 1. *J Clin Oncol* 2009;27:5800–7.
9. Murakami H, Doi T, Yamamoto N, et al. Phase 1 study of ganitumab (AMG 479), a fully human monoclonal antibody against the insulin-like growth factor receptor type 1 (IGF 1R), in Japanese patients with advanced solid tumors. *Cancer Chemother Pharmacol* 2012;70:407–14.
10. Kindler HL, Richards DA, Garbo LE, et al. A randomized, placebo-controlled phase 2 study of ganitumab (AMG 479) or conatumumab (AMG 655) in combination with gemcitabine in patients with metastatic pancreatic cancer. *Ann Oncol* 2012;23:2834–42.
11. Lu JF, Deng H, Tang R, et al. Exposure–response analysis to facilitate phase 3 dose selection for ganitumab (AMG 479) in combination with gemcitabine to treat metastatic pancreatic cancer. ASCO 47th Annual Meeting, Chicago, IL, June 3–7, abstract 4049, 2011.
12. Therasse P, Arbuck SG, Eisenhauer EA, et al. New guidelines to evaluate the response to treatment in solid tumours. *J Natl Cancer Inst* 2000;92:205–16.
13. Okada S, Ueno H, Okusaka T, Ikeda M, Furuse J, Maru Y. Phase I trial of gemcitabine in patients with advanced pancreatic cancer. *Jpn J Clin Oncol* 2001;31:7–12.
14. Scagliotti GV, Novello S. The role of the insulin-like growth factor signaling pathway in non-small cell lung cancer and other solid tumors. *Cancer Treat Rev* 2012;38:292–302.
15. Barrenäs M, Landin-Wilhelmsen K, Hanson C. Ear and hearing in relation to genotype and growth in Turner syndrome. *Hear Res* 2000;144:21–8.

Am J Clin Dermatol
DOI 10.1007/s40257-015-0116-x

ORIGINAL RESEARCH ARTICLE

Efficacy of Prophylactic Minocycline Treatment for Skin Toxicities Induced by Erlotinib Plus Gemcitabine in Patients with Advanced Pancreatic Cancer: A Retrospective Study

Akira Shinohara · Masafumi Ikeda · Hiroyuki Okuyama · Misaki Kobayashi · Hideki Funazaki · Shuichi Mitsunaga · Satoshi Shimizu · Izumi Ohno · Hideaki Takahashi · Yasuhiko Ichida · Kunio Takahashi · Takuji Okusaka · Shinichiro Saitoh

Abstract

Background Erlotinib has been reported as being associated with a high incidence of skin toxicities such as acneiform rash, paronychia, and xerosis.

Objective The aim of this study was to evaluate the efficacy of prophylactic minocycline treatment for the skin toxicities induced by erlotinib as compared with deferred minocycline treatment in patients with pancreatic cancer treated with erlotinib plus gemcitabine.

Methods A total of 96 patients were studied retrospectively, of whom 44 received prophylactic minocycline between August 2012 and June 2013 and 52 received deferred minocycline treatment between August 2011 and July 2012 at the National Cancer Center Hospital East, Kashiwa, Japan. In the prophylactic minocycline group, 200 mg/day oral minocycline was prophylactically administered during the treatment period.

Results The incidence rate of acneiform rash and xerosis of any grade during the first 6 weeks of treatment was significantly reduced in the prophylactic minocycline group compared with the deferred minocycline treatment group (47.7 vs. 80.8 %, $p < 0.001$; 2.3 vs. 19.2 %, $p = 0.01$). Multivariate analysis identified prophylactic minocycline as a significant independent factor associated with the incidence of acneiform rash and xerosis of any severity (odds ratio [OR] 0.16, 95 % confidence interval [CI] 0.06–0.46, $p < 0.001$; OR 0.11, 95 % CI 0.01–0.90, $p = 0.04$).

Conclusion Prophylactic minocycline appears to be useful for the management of erlotinib-related acneiform rash and xerosis during chemotherapy in patients with advanced pancreatic cancer.

Key Points

Skin toxicities induced by erlotinib, a small-molecular tyrosine kinase inhibitor of epidermal growth factor receptor (EGFR), impair quality of life and often necessitate treatment interruption, dose reduction, and discontinuation of treatment.

Tetracycline may have anti-inflammatory effect in addition to its antimicrobial effect.

Prophylactic minocycline appears to be useful for the management of erlotinib-related acneiform rash and xerosis.

1 Introduction

In recent years, epidermal growth factor receptor (EGFR) has become an important target for therapy in a variety of cancers. Erlotinib, a small-molecular tyrosine kinase inhibitor of EGFR, administered in combination with gemcitabine has been shown to significantly improve overall

A. Shinohara · M. Kobayashi · H. Funazaki · Y. Ichida · K. Takahashi · S. Saitoh
Department of Pharmacy, National Cancer Center Hospital East, Kashiwa, Japan

M. Ikeda (✉) · H. Okuyama · S. Mitsunaga · S. Shimizu · I. Ohno · H. Takahashi
Department of Hepatobiliary and Pancreatic Oncology, National Cancer Center Hospital East, 6-5-1 Kashiwanoha, Kashiwa, Chiba 277-8577, Japan
e-mail: masikeda@east.ncc.go.jp

T. Okusaka
Department of Hepatobiliary and Pancreatic Oncology, National Cancer Center Hospital, Tokyo, Japan

Published online: 17 February 2015

survival (OS) compared with gemcitabine alone in patients with advanced pancreatic cancer [1]. However, treatment with erlotinib plus gemcitabine has been reported as being associated with the development of an acneiform rash in approximately 70 % of patients [1, 2]. Erlotinib has also been reported as inducing paronychia and xerosis [3, 4]. Severe skin toxicity may impact the efficacy of chemotherapy combined with EGFR-targeted drugs by necessitating treatment interruption, dose reductions, and discontinuation of therapy. In addition, these skin toxicities may also impair the quality of life (QOL) of patients with advanced pancreatic cancer. Therefore, appropriate management of the skin toxicities induced by EGFR inhibitors is essential during combined treatment with chemotherapy in patients with advanced pancreatic cancer.

Tetracycline is a well known antimicrobial drug, but it is also often used to treat the skin toxicities induced by EGFR inhibitors. The efficacy of systemic tetracycline therapy combined with topical moisturizers and/or steroids has been reported for the skin toxicities, including acneiform rash, paronychia, and xerosis, induced by EGFR inhibitors [5, 6]. Thus, tetracycline may also have an anti-inflammatory effect in addition to its antimicrobial effect.

We initially introduced deferred minocycline treatment, initiated after the emergence of grade 2 or 3 skin toxicities, for patients with advanced pancreatic cancer receiving erlotinib plus gemcitabine treated between August 2011 and July 2012. However, skin toxicities induced by erlotinib in patients with advanced pancreatic cancer impaired patients' QOL and often necessitated treatment interruption, dose reductions, and discontinuation of therapy. Therefore, in August 2012, we introduced prophylactic minocycline treatment for the skin toxicities induced by erlotinib in patients with advanced pancreatic cancer. The objective of this study was to retrospectively analyze data from these two patient groups in order to evaluate the efficacy of prophylactic minocycline treatment for the skin toxicities induced by erlotinib as compared with deferred minocycline treatment in patients with advanced pancreatic cancer receiving treatment with erlotinib plus gemcitabine.

2 Methods

This retrospective study was conducted with the approval of the ethics committee of the National Cancer Center, and in accordance with epidemiological research guidelines (2013-126).

2.1 Patients

Study subjects were patients with advanced pancreatic cancer treated with erlotinib plus gemcitabine for more than 6 weeks at the National Cancer Center Hospital East, Kashiwa, Japan, between August 2011 and June 2013. Patients who did not receive erlotinib plus gemcitabine for more than 6 weeks were excluded from this study, because they had limited chance to develop erlotinib-related skin toxicities. Erlotinib was administered at a dose of 100 mg daily, and gemcitabine was administered intravenously over 30 min at a dose of 1,000 mg/m^2 once every week for 3 consecutive weeks; each treatment cycle lasted for 4 weeks. The doses of erlotinib and gemcitabine could be adjusted based on the development of adverse events. The treatment was continued unless disease progression became obvious or unacceptable toxicity occurred.

2.2 Skin Treatment Schedule

A total of 96 patients were treated with erlotinib plus gemcitabine between August 2011 and June 2013 at our hospital. Among them, 44 patients treated between August 2012 and June 2013 received prophylactic minocycline treatment, and 52 patients treated between August 2011 and July 2012 received deferred minocycline treatment (Fig. 1). In the prophylactic minocycline group, 200 mg/day oral minocycline was administered from day 1 of chemotherapy and continued. In the deferred minocycline treatment group, 200 mg/day oral minocycline was initiated after the emergence of grade 2 or 3 skin toxicities, in principle. In both groups, emollients such as heparinoids were applied to the susceptible regions (e.g., face, chest, and back) and portions of the skin that dry easily (e.g., hands and feet) from day 1, and skin treatment with topical steroids of strong and medium classes was initiated after the emergence of any skin toxicities. The steroids difluprednate 0.05 % and hydrocortisone butyrate 0.1 % were applied to the body and face, respectively.

2.3 Erlotinib and Gemcitabine Relative Dose Intensity

Erlotinib dose intensity was defined as the cumulative dose received divided by the duration of the study therapy in weeks. Erlotinib relative dose intensity was defined as the dose intensity divided by the dose prescribed for the duration of the first 6 weeks of erlotinib administration (100 mg $\times$ the number of days that a patient received treatment).

The total administered doses of gemcitabine were calculated as the total delivered dose of gemcitabine divided by the body surface area (mg/m^2). Gemcitabine dose intensity was defined as the total administered doses divided by the duration of the study therapy in weeks. Gemcitabine relative dose intensity was defined as the dose intensity divided by planned dose intensity for the duration of the first 6 weeks.

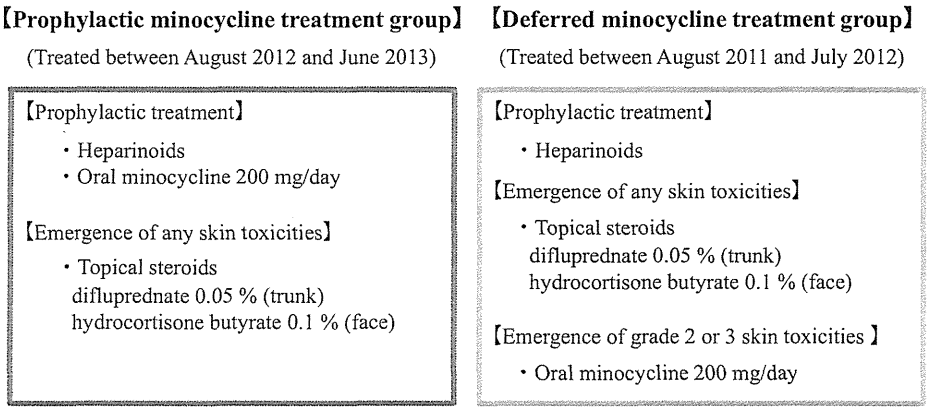

Fig. 1 Treatment protocols in the prophylactic and deferred minocycline treatment groups

2.4 Statistical Analysis

All adverse events, including acneiform rash, paronychia, and xerosis were graded according to the Common Toxicity Criteria for Adverse Events (CTCAE, version 4.0). Skin toxicities were evaluated during the first 6 weeks of erlotinib plus gemcitabine treatment. Time to first occurrence of acneiform rash was defined as the period from the commencement of treatment to the date of the first occurrence of acneiform rash. Responses and progression were evaluated using the Response Evaluation Criteria in Solid Tumors (RECIST version 1.1). OS was determined as the period from the commencement of treatment to the date of death from any cause or the date of the last follow-up. Progression-free survival (PFS) was defined as the period from the commencement of treatment to the date of confirmation of disease progression or death. Time to first occurrence of skin toxicity, OS, and PFS were calculated by the Kaplan–Meier product-limit method. The cut-off for the follow-up data was 30 June 2013.

Univariate and multivariate analyses were undertaken to evaluate the relationships between the pretreatment clinical variables and the risk of development of acneiform rash and xerosis. The variables were selected by considering their possible relationships to the incidence of skin rash observed in our own clinical experience or in previous reports [7–9]. The univariate associations between the incidence of skin rash and the pretreatment clinical variables were tested using the χ^2 test or Fisher's exact test. We entered factors identified as significant by univariate analysis with a significance level of <0.2 into the multivariate analysis. Multivariate analysis was undertaken using logistic regression to identify significant factors associated with the incidence of acneiform rash of any grade. We used SPSS software (version 17.00, SPSS, Inc., Chicago, IL, USA) for the statistical analysis. p values <0.05 were considered to indicate statistical significance.

Table 1 Patient characteristics

Variable	Prophylactic minocycline treatment	Deferred minocycline treatment	p value
No. of patients	44	52	
Age, years	66 (41–82)	67 (34–83)	0.40
Gender			
Female	16 (36.4)	23 (44.2)	
Male	28 (63.6)	29 (55.8)	0.33
UICC disease stage			
III	8 (18.2)	12 (23.1)	
IV	36 (81.8)	40 (76.9)	0.72
Primary tumor site			
Body or tail of pancreas	29 (65.9)	30 (57.7)	
Head of pancreas	15 (34.1)	22 (42.3)	0.41
Ascites present	18 (40.9)	16 (30.8)	0.45
ECOG PS			
0	26 (59.1)	35 (67.3)	
1	18 (40.9)	15 (28.8)	
≥2	0 (0)	2 (3.8)	0.23
Prior surgical resection of primary tumor	2 (4.5)	3 (5.8)	0.58
CEA (ng/mL)	6.4 (0.4–80.3)	4.2 (0.5–293.4)	0.33
CA19-9 (U/mL)	658 (0.1–98,500)	506.9 (0.1–453,000)	0.17

Data are presented as n (%) or median (range) unless otherwise indicated

CA19-9 carbohydrate antigen 19-9, *CEA* carcinoembryonic antigen, *ECOG PS* Eastern Cooperative Oncology Group performance status, *UICC* Union for International Cancer Control

3 Results

3.1 Patient Characteristics

The baseline characteristics of the study subjects are summarized in Table 1. No significant differences were

Table 2 Incidence of skin toxicities during the first 6 weeks of treatment with erlotinib plus gemcitabine

Variables	Prophylactic minocycline treatment	Deferred minocycline treatment	*p* value
Acneiform rash			
Any grade	21 (47.7)	42 (80.8)	<0.001
Grade ≥2	9 (20.5)	15 (28.8)	0.34
Paronychia			
Any grade	7 (15.9)	11 (21.2)	0.51
Grade ≥2	3 (6.8)	3 (5.8)	0.58
Xerosis			
Any grade	1 (2.3)	10 (19.2)	0.01
Grade ≥2	0 (0)	0 (0)	–
ERL dose intensity during first 6 weeks of tx with ERL plus GEM	83.3 % (14.3–100)	83.3 % (4.8–100)	0.49
GEM dose intensity during first 6 weeks of tx with ERL plus GEM	80.7 % (35.4–100)	77.0 % (37.9–100)	0.57

Data are presented as *n* (%) or mean (range) unless otherwise indicated

ERL erlotinib, *GEM* gemcitabine, *tx* treatment

observed in the baseline characteristics between the prophylactic minocycline treatment group and the deferred minocycline treatment group. The median duration of erlotinib treatment during the first 6 weeks of chemotherapy was 5.1 and 5.2 weeks in the prophylactic and deferred minocycline treatment groups, respectively ($p = 0.66$). No significant differences were observed in the proportion of erlotinib treatment interruption between the prophylactic and the deferred minocycline treatment groups (56.8 vs. 57.7 %; $p = 0.93$). The proportion of erlotinib dose reduction tended to be lower in the prophylactic than the deferred minocycline treatment group, although it was not significant (6.8 vs. 17.3 %; $p = 0.12$). No patients in the prophylactic minocycline treatment group required erlotinib dose reduction for skin toxicities; however, three patients in the deferred group did.

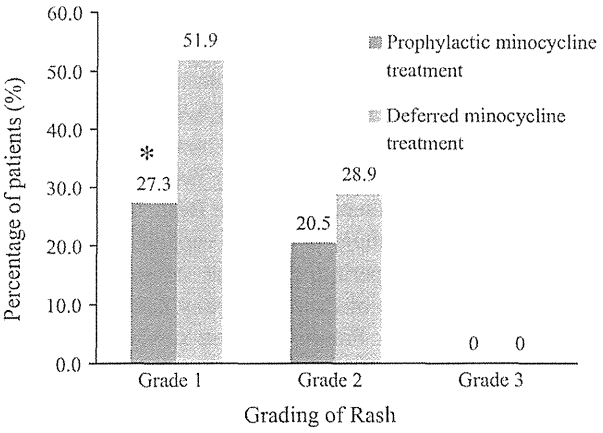

Fig. 2 Incidence of acneiform rash of each grade of severity in the prophylactic minocycline treatment group and deferred minocycline treatment group. *$p = 0.01$

3.2 Efficacy of Prophylactic Minocycline Treatment

The incidence rate of acneiform rash of any grade was significantly lower in the prophylactic than in the deferred minocycline treatment group (47.7 vs. 80.8 %; $p < 0.001$; Table 2). The incidence rate of acneiform rash of grade 1 severity was significantly lower in the prophylactic than in the deferred minocycline treatment group (27.3 vs. 51.9 %, $p = 0.01$) (Fig. 2). However, the incidence rate of acneiform rash of grade 2 severity was not significantly lower in the prophylactic than in the deferred minocycline treatment group (20.5 vs. 28.9 %, $p = 0.34$) (Fig. 2). In addition, the incidence rate of xerosis of any grade was also significantly lower in the prophylactic than in the deferred minocycline treatment group (2.3 vs. 19.2 %; $p = 0.01$). However, no significant difference was observed in the incidence rate of paronychia of any grade between the two treatment groups.

The median time to first occurrence of acneiform rash was 2.0 weeks (95 % confidence interval [CI] 1.4–2.6) in the deferred minocycline treatment group (hazard ratio [HR] 0.43; 95 % CI 0.26–0.73, $p < 0.001$) (Fig. 3). This was not reached in the prophylactic minocycline treatment group.

3.3 Risk Factors for the Development of Acneiform Rash and Xerosis

To identify risk factors for the development of acneiform rash and xerosis, associations between the incidence of acneiform rash or xerosis and patient characteristics were analyzed via univariate analysis (Table 3). The analysis identified prophylactic minocycline treatment as a significant factor associated with the incidence of acneiform rash ($p < 0.001$). In addition, the incidence rate of

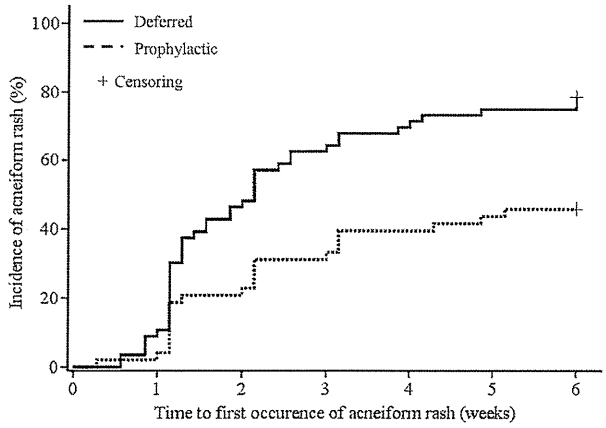

Fig. 3 Time to first occurrence of acneiform rash of any grade of severity in the prophylactic minocycline treatment group and deferred minocycline treatment group during the first 6 weeks of treatment. Median time to first occurrence of acneiform rash was not reached in the prophylactic minocycline treatment group, as compared with the median time to first occurrence of rash of 2.0 weeks (95 % confidence interval 1.4–2.6) in the deferred minocycline treatment group (hazard ratio 0.43; 95 % confidence interval 0.26–0.73; $p < 0.001$)

acneiform rash was numerically lower in the female (55.0 %) versus male (73.2 %) group ($p = 0.06$); in the group receiving a lower dose intensity of erlotinib (57.5 %) versus the higher-dose intensity group (71.4 %; $p = 0.16$); in the group with Union for International Cancer Control (UICC) stage IV disease (61.0 %) versus those with stage III (84.2 %; $p = 0.06$); and in the group with Eastern Cooperative Oncology Group (ECOG) performance status ≥ 2 (0 %) versus those with performance status 0–1 (67.0 %; $p = 0.12$) (Table 3).

Prophylactic minocycline treatment (odds ratio [OR] 0.16; 95 % CI 0.06–0.46; $p < 0.001$) and female gender (OR 0.30; 95 % CI 0.11–0.87; $p = 0.03$) were factors significantly associated with the incidence of acneiform rash in the multivariate logistic regression analysis (Table 4).

In addition, prophylactic minocycline treatment ($p = 0.01$) was also identified via univariate analysis as a factor significantly associated with the incidence of xerosis. The incidence rate of xerosis was numerically lower in the group with higher levels of serum carcinoembryonic antigen (CEA) (6.7 vs. 15.7 % in the group with lower serum levels; $p = 0.17$) (Table 3). Multivariate logistic regression analysis also identified prophylactic minocycline treatment as a significant independent factor associated with the incidence of xerosis (OR 0.11; 95 % CI 0.01–0.90; $p = 0.04$; Table 4).

3.4 Antitumor Efficacy

The response rate was 9.1 % in the prophylactic and 8.0 % in the deferred minocycline treatment group ($p = 0.85$). The disease control rate was also similar between the two groups (86.4 vs. 84.0 %, respectively; $p = 0.75$). The median OS was 18.0 months (95 % CI 9.5–26.5) in the deferred minocycline treatment group (HR 0.69; 95 % CI 0.30–1.57; $p = 0.38$) and was not reached in the prophylactic minocycline treatment group. The OS rates at 6 months were 76.2 % (95 % CI 60.4–92.1) in the prophylactic minocycline treatment group and 88.1 % (95 % CI 50.9–97.1) in the deferred treatment group. The median PFS time was 5.4 months (95 % CI 4.5–6.2) in the prophylactic group and 5.7 months (95 % CI 3.3–8.2) in the deferred group (HR 0.86; 95 % CI 0.51–1.47; $p = 0.59$).

3.5 Safety

The adverse events in the treatment period overall are summarized in Table 5. No significant differences were observed in adverse effects, excluding skin toxicities, between the two groups. In particular, the incidence of nausea, vomiting, vertigo, and liver dysfunction, which are known adverse events associated with the administration of minocycline, were similar between the groups.

4 Discussion

Skin toxicities, including acneiform rash, paronychia, and xerosis, are the most frequent adverse effects associated with the administration of EGFR inhibitors [1, 2, 10, 11]. Because neither univariate nor multivariate analysis identified the dose intensity of gemcitabine as a significant independent factor associated with the incidence of acneiform rash or xerosis of any grade of severity, skin toxicities seemed to be unrelated to the gemcitabine treatment. These skin toxicities may impair the QOL of patients and cause treatment interruption, dose reductions, or discontinuation of EGFR-targeted therapy, although they are not life-threatening toxicities. EGFR is normally expressed in undifferentiated, proliferating keratinocytes in the basal and suprabasal layers of the epidermis and regulate normal keratinocyte proliferation, differentiation, migration, and survival [12, 13]. Thus, the skin toxicities induced by EGFR inhibitors appear to involve inflammatory changes in the follicular epithelium [14, 15], although the mechanism is still not fully understood. Tetracyclines are antibacterial drugs; however, several studies suggest that they may also have anti-inflammatory effects. Inhibition of the secretion of tumor necrosis factor (TNF)-α and interleukin (IL)-6, phospholipase A_2, nitric oxide synthases, and/or caspase-1 by tetracyclines, with modulation of lymphocyte proliferation, neutrophil migration, and phagocytosis, may represent the mechanisms underlying

Table 3 Univariate analysis to identify possible factors related to the development of acneiform rash and xerosis during the first 6 weeks of treatment with erlotinib plus gemcitabine

Variables	*n*	Pts with acneiform rash	Pts without acneiform rash	*p* value	Pts with xerosis	Pts without xerosis	*p* value
Minocycline treatment							
Prophylactic	44	21 (47.7)	23 (52.3)		1 (2.3)	43 (97.7)	
Deferred	52	42 (80.8)	10 (19.2)	<0.001	10 (19.2)	42 (80.8)	0.01
Gender							
Female	40	22 (55.0)	18 (45.0)		6 (15.0)	34 (85.0)	
Male	56	41 (73.2)	15 (26.8)	0.06	5 (8.9)	51 (91.1)	0.27
Age, years							
<70	40	25 (62.5)	15 (37.5)		4 (10.0)	36 (90.0)	
≥70	56	38 (67.9)	18 (32.1)	0.59	7 (12.5)	49 (87.5)	0.48
BSA (m^2)							
<1.585 (median)	49	19 (38.8)	30 (61.2)		7 (14.3)	42 (85.3)	
≥1.585 (median)	47	14 (29.8)	33 (70.2)	0.35	4 (8.5)	43 (91.5)	0.38
Dose intensity of ERL (%)							
<83.3 (median)	40	23 (57.5)	17 (42.5)		3 (7.5)	37 (92.5)	
≥83.3 (median)	56	40 (71.4)	16 (28.6)	0.16	8 (14.3)	48 (85.7)	0.24
Dose intensity of GEM (%)							
<79.4 (median)	47	33 (70.2)	14 (29.8)		7 (14.9)	40 (85.1)	
≥79.4 (median)	49	30 (61.2)	19 (38.7)	0.35	4 (8.2)	45 (91.8)	0.24
UICC disease stage							
III	19	16 (84.2)	9 (47.4)		3 (15.8)	16 (84.2)	
IV	77	47 (61.0)	30 (38.9)	0.06	8 (10.4)	69 (89.6)	0.38
Primary tumor site							
Body or tail of pancreas	59	37 (62.7)	22 (37.3)		6 (10.2)	53 (89.8)	
Head of pancreas	37	26 (70.3)	11 (29.7)	0.45	5 (13.5)	32 (86.5)	0.43
Ascites							
Present	29	17 (58.6)	12 (41.4)		2 (6.9)	27 (93.1)	
Absent	67	46 (68.7)	21 (31.3)	0.34	9 (13.4)	58 (86.6)	0.29
ECOG PS							
0–1	94	63 (67.0)	31 (33.0)		11 (11.7)	83 (88.3)	
≥2	2	0 (0)	2 (100)	0.12	0 (0)	2 (100)	0.78
CEA (ng/mL)							
<5.25 (median)	51	35 (68.6)	16 (31.4)		8 (15.7)	43 (84.3)	
≥5.25 (median)	45	28 (62.2)	17 (37.8)	0.51	3 (6.7)	42 (93.3)	0.17
CA19-9 (U/mL)							
<658 (median)	51	36 (70.6)	15 (29.4)		6 (11.8)	45 (88.2)	
≥658 (median)	45	27 (60.0)	18 (40.0)	0.28	5 (11.1)	40 (88.9)	0.92

Data are presented as *n* (%) unless otherwise indicated

BSA body surface area, *CA19-9* carbohydrate antigen 19-9, *CEA* carcinoembryonic antigen, *ECOG PS* Eastern Cooperative Oncology Group performance status, *ERL* erlotinib, *GEM* gemcitabine, *pts* patients, *UICC* Union for International Cancer Control

the anti-inflammatory effect of tetracyclines [16–19]. In addition, there were almost no minocycline-related adverse effects in this study. Based on these findings, we theorized that we could effectively counteract the inflammatory changes in the follicular epithelium with prophylactic systemic tetracycline treatment.

In this retrospective analysis, we clarified that prophylactic oral minocycline treatment significantly reduced the incidence of acneiform rash and xerosis induced by erlotinib in patients with advanced pancreatic cancer. Furthermore, no significant differences between the two groups were observed in the incidence of nausea, vomiting,

Table 4 Multivariate logistic regression analysis to identify possible factors related to the development of acneiform rash and xerosis during the first 6 weeks of treatment with erlotinib plus gemcitabine

Factors	Acneiform rash		Xerosis	
	OR (95 % CI)	*p* value	OR (95 % CI)	*p* value
Minocycline treatment				
Prophylactic	0.16 (0.06–0.46)	<0.001	0.11 (0.01–0.90)	0.04
Deferred	1		1	
Gender				
Female	0.30 (0.11–0.87)	0.03		
Male	1			
Erlotinib dose intensity (%)				
<83.3	0.61 (0.23–1.65)	0.30		
≥83.3	1			
UICC disease stage				
III	4.05 (0.94–17.53)	0.06		
IV	1			
ECOG PS				
≥2	1.54 (0.62–3.83)	0.35		
0–1	1			
CEA (ng/mL)				
<5.25			0.50 (0.12–2.10)	0.34
≥5.25			1	

CEA carcinoembryonic antigen, *CI* confidence interval, *ECOG PS* Eastern Cooperative Oncology Group performance status, *OR* odds ratio, *UICC* Union for International Cancer Control

vertigo, and liver dysfunction, known adverse events associated with minocycline treatment. Therefore, our results suggest that long-term treatment with 200 mg/day minocycline, which is the generally used dose around the world, was effective and feasible in patients with advanced pancreatic cancer undergoing treatment with erlotinib plus gemcitabine. In addition, no significant difference was observed in response rate, disease control rate, or PFS between the prophylactic and the deferred minocycline treatment groups in this study. Thus, prophylactic minocycline treatment did not appear to have a significant impact on the anti-tumor effects of erlotinib plus gemcitabine.

Two studies have shown the anti-inflammatory effects of tetracycline following systemic administration [5, 6]. In particular, the open-label phase II STEPP (Skin Toxicity Evaluation Protocol with Panitumumab) trial reported the most persuasive results [6]. It demonstrated that prophylactic skin treatment with a skin moisturizer, sunscreen, topical steroid, and oral doxycycline significantly reduced the incidence of grade 2 or worse skin toxicities compared with the deferred treatment group in metastatic colorectal cancer patients treated with panitumumab (29 vs. 62 %; OR 0.3; 95 % CI 0.1–0.6). Because the prophylactic skin treatment in the STEPP trial included various skincare agents, it is impossible to evaluate the individual efficacy of each of these skincare agents. On the other hand, we could evaluate the efficacy of prophylactic minocycline treatment, because the only difference between the prophylactic and deferred minocycline treatment groups was in the use of minocycline. However, this study was a small, non-randomized, retrospective comparative study, and the patient groups were not concurrently treated. Our results may not be generalizable to the entire patient population because of the single-center setting of the study. A well designed, randomized controlled trial of minocycline is mandatory to evaluate the effects of tetracyclines for the skin toxicities induced by erlotinib in patients with pancreatic cancer.

This retrospective study demonstrated the effectiveness of prophylactic oral minocycline treatment for preventing the development of acneiform rash and xerosis during treatment with erlotinib and gemcitabine in patients with advanced pancreatic cancer; however, the treatment failed to prevent the development of paronychia. A few case reports suggest the efficacy of doxycycline for the treatment of paronychia induced by EGFR inhibitors [20]; however, no randomized controlled trials have shown the efficacy of tetracycline for preventing paronychia induced by EGFR inhibitors. Therefore, there is a need to establish therapies for paronychia in the future.

In our study, and consistent with previous reports, multivariate analysis identified female gender as a significant independent factor associated with the incidence of acneiform rash [9, 21]. Migliaccio et al. [22, 23] reported that activation of Src triggered by androgens induces EGFR phosphorylation. This hormonal action may be one of the reasons for the difference in the incidence of acneiform rash between male and female patients.

Table 5 Treatment-emergent toxicities occurring during the first 6 weeks of treatment with erlotinib plus gemcitabine

Variables	Prophylactic minocycline treatment		Deferred minocycline treatment		*p* value (any grade)	*p* value (grade ≥3)
	Any	Grade ≥3	Any	Grade ≥3		
Any toxicity	44 (100)	25 (56.8)	52 (100)	36 (69.2)	–	0.21
Hematologic						
Leukocytes	41 (93.2)	12 (27.3)	47 (90.4)	16 (30.8)	0.46	0.71
Neutropenia	39 (88.6)	18 (40.9)	44 (84.6)	23 (44.2)	0.24	0.74
Hemoglobin	31 (70.5)	4 (9.1)	42 (80.8)	10 (19.2)	0.60	0.16
Platelets	35 (79.6)	4 (9.1)	39 (75.0)	5 (9.6)	0.61	0.61
Non-hematologic						
Nausea	26 (59.1)	0 (0)	24 (46.2)	0 (0)	0.21	–
Vomiting	9 (20.5)	0 (0)	7 (13.5)	0 (0)	0.36	–
Diarrhea	14 (31.8)	0 (0)	16 (30.8)	0 (0)	0.91	–
Fatigue	29 (65.9)	2 (4.6)	31 (59.6)	1 (1.9)	0.53	0.44
Vertigo	3 (6.8)	0 (0)	1 (1.9)	0 (0)	0.25	–
ILD-like syndrome	2 (4.6)	0 (0)	5 (9.6)	1 (1.9)	0.15	0.54
Biochemical						
AST	28 (63.6)	6 (13.6)	32 (61.5)	7 (13.5)	0.83	0.98
ALT	23 (52.3)	6 (13.6)	29 (55.8)	8 (15.4)	0.73	0.81
Bilirubin	18 (40.9)	4 (9.1)	22 (42.3)	4 (7.7)	0.89	0.55
ALP	16 (31.8)	1 (2.3)	19 (36.5)	0 (0)	0.63	0.46
Creatinine	14 (31.8)	0 (0)	21 (40.4)	0 (0)	0.39	–

Data are presented as *n* (%) unless otherwise indicated

ALP alkaline phosphatase, *ALT* alanine aminotransferase, *AST* aspartate aminotransferase, *ILD* interstitial lung disease

5 Conclusions

In conclusion, in our retrospective analysis, prophylactic oral minocycline treatment significantly reduced the incidence of acneiform rash and xerosis, but not that of paronychia, induced by erlotinib during erlotinib plus gemcitabine treatment in patients with advanced pancreatic cancer. This finding should be confirmed in future randomized controlled studies. Prophylactic minocycline treatment appears to be useful for the management of erlotinib-related acneiform rash and xerosis during treatment with erlotinib plus gemcitabine in patients with advanced pancreatic cancer.

Acknowledgments This manuscript was prepared without the help of any funding source. A. Shinohara, M. Ikeda, H. Okuyama, M. Kobayashi, H. Funazaki, S. Mitsunaga, S. Shimizu, I. Ohno, H. Takahashi, Y. Ichida, K. Takahashi, T. Okusaka and S. Saitoh have no conflicts of interests to declare.

References

1. Moore MJ, Goldstein D, Hamm J, Figer A, et al. Erlotinib plus gemcitabine compared with gemcitabine alone in patients with advanced pancreatic cancer: a phase III trial of the national cancer institute of canada clinical trial group. J Clin Oncol. 2007;25:1960–6.
2. Okusaka T, Furuse J, Funakoshi A, et al. Phase II study of erlotinib plus gemcitabine in Japanese patients with unresectable pancreatic cancer. Cancer Sci. 2011;102:425–31.
3. Nakagawa K, Kudoh S, Ohe Y, et al. Postmarketing surveillance study of erlotinib in Japanese patients with non-small-cell lung cancer (NSCLC): an interim analysis of 3488 patients (POLARSTAR). J Thorac Oncol. 2012;7:1296–303.
4. Galimont-Collen AF, Vos LE, Lavrijsen AP, et al. Classification and management of skin, hair, nail and mucosal side-effects of epidermal growth factor receptor (EGFR) inhibitors. Eur J Cancer. 2007;43:845–51.
5. Scope A, Agero AL, Dusza SW, et al. Randomized double-blind trial of prophylactic oral minocycline and topical tazarotene for cetuximab-associated acne-like eruption. J Clin Oncol. 2007;25:5390–6.
6. Lacouture ME, Michell EP, Piperdi B, et al. Skin toxicity evaluation protocol with panitumumab (STEPP), a phase II, open-label, randomized trial evaluating the impact of a pre-emptive skin treatment regimen on skin toxicities and quality of life in patients with metastatic colorectal cancer. J Clin Oncol. 2010;28:1351–7.
7. Wacker B, Nagrani T, Weinberg J, et al. Correlation between development of rash and efficacy in patients treated with the epidermal growth factor receptor tyrosine kinase inhibitor erlotinib in two large phase III studies. Clin Cancer Res. 2007;13:3913–21.
8. Wheatley-Price P, Ding K, Seymour L, et al. Erlotinib for advanced non-small-cell lung cancer in the elderly: an analysis of

the National Cancer Institute of Canada Clinical Trials Group study BR.21. J Clin Oncol. 2008;26:2350–7.
9. Jatoi A, Green EM, Rowland KM, et al. Clinical predictors of severe cetuximab-induced rash: observation from 933 patients enrolled in North Central Cancer Treatment Group study N0147. Oncology. 2009;77:120–3.
10. Perez-Soler R, Chachoua A, Hammond LA, et al. Determinations of tumor response and survival with erlotinib in patients with non-small-cell lung cancer. J Clin Oncol. 2004;22:3238–47.
11. Soulieres D, Senzer NN, Vokes EE, et al. Multicenter phase II study of erlotinib, an oral epidermal growth factor receptor tyrosine kinase inhibitor, in patients with recurrent or metastatic squamous cell cancer of the head and neck. J Clin Oncol. 2004;22:3238–47.
12. Nanney LB, Stoscheck CM, King LE Jr, et al. Immunolocalization of epidermal growth factor receptors in normal developing human skin. J Invest Dermatol. 1990;94:742–8.
13. Li T, Perez-Soler R. Skin toxicities associated with epidermal growth factor receptor inhibitors. Targ Oncol. 2009;4:107–19.
14. Pastore S, Mascia F, Mariotti F, et al. ERK1/2 regulates epidermal chemokine expression and skin inflammation. J Immunol. 2005;174:5047–56.
15. Lacouture ME. Mechanisms of cutaneous toxicities to EGFR inhibitors. Nat Rev Cancer. 2006;6:803–12.
16. Pruzanski W, Greenwald RA, Street IP, et al. Inhibition of enzymatic activity of phospholipases A2 by minocycline and doxycycline. Biochem Pharmacol. 1992;44:1165–70.
17. Amin AR, Attur MG, Thakker GD, et al. A novel mechanism of action of tetracyclines: effects on nitric oxide synthases. Proc Natl Acad Sci. 1996;93:14014–9.
18. Dreno B, Bettoli V, Ochsendorf F, et al. European recommendations on the use of oral antibiotics for acne. Eur J Dermatol. 2004;14:391–9.
19. Vincent JA, Mohr S. Inhibition of caspase-1/interleukin-1beta signaling prevents degeneration of retinal capillaries in diabetes and galactosemia. Diabetes. 2007;56:224–30.
20. Shu KY, Kindler HL, Medenica M, et al. Doxycycline for the treatment of paronychia induced by the epidermal growth factor receptor inhibitor cetuximab. Br J Dermatol. 2006;154:191–2.
21. Stintzing S, Kapaun C, Laubender RP, et al. Prognostic value of cetuximab-related skin toxicity in metastatic colorectal cancer patients and its correlation with parameters of the epidermal growth factor receptor signal transduction pathway: results from a randomized trial of the GERMAN AIO CRC Study Group. Int J Cancer. 2013;132:236–45.
22. Migliaccio A, Castoria G, Di Domenico M, et al. Steroid-induced androgen receptor-oestradiol receptor-Src complex triggers prostate cancer cell proliferation. EMBO J. 2000;19:5406–17.
23. Migliaccio A, Castoria G, Di Domenico M, et al. Crosstalk between EGFR and extranuclear steroid receptors. Ann NY Acad Sci. 2006;1089:194–200.

OPEN

Therapeutic Priority of the PI3K/AKT/mTOR Pathway in Small Cell Lung Cancers as Revealed by a Comprehensive Genomic Analysis

Shigeki Umemura, MD, PhD, Sachiyo Mimaki, MS, † Hideki Makinoshima, PhD, † Satoshi Tada, MS, † Genichiro Ishii, MD, PhD,‡ Hironobu Ohmatsu, MD,* Seiji Niho, MD, PhD,* Kiyotaka Yoh, MD,*,† Shingo Matsumoto, MD, PhD,*,† Akiko Takahashi, MD,* Masahiro Morise, MD, PhD,* Yuka Nakamura, BS,‡ Atsushi Ochiai, MD, PhD,‡ Kanji Nagai, MD, PhD,§ Reika Iwakawa, PhD,‖ Takashi Kohno, PhD,‖ Jun Yokota, MD, PhD,‖ Yuichiro Ohe, MD, PhD,* Hiroyasu Esumi, MD, PhD,† Katsuya Tsuchihara, MD, PhD,† and Koichi Goto, MD, PhD,**

Introduction: The information regarding therapeutically relevant genomic alterations in small cell lung cancer (SCLC) is not well developed. We analyzed the SCLC genome using an integrative approach to stratify the targetable alterations.

Methods: We performed whole exon sequencing ($n = 51$) and copy number analysis ($n = 47$) on surgically resected tumors and matched normal tissue samples from treatment-naive Japanese SCLC patients.

Results: The demographics of the 51 patients included in this study were as follows: median age, 67 years (range, 42–86 years); female, 9 (18%); history of smoking, 50 (98%); and pathological stage I/II/III/IV, 28/13/9/1, respectively. The average number of nonsynonymous mutations was 209 (range, 41–639; standard deviation, 130). We repeatedly confirmed the high prevalence of inactivating mutations in *TP53* and *RB1*, and the amplification of *MYC* family members. In addition, genetic alterations in the PI3K/AKT/mTOR pathway were detected in 36% of the tumors: *PIK3CA*, 6%; *PTEN*, 4%; *AKT2*, 9%; *AKT3*, 4%; *RICTOR*, 9%; and *mTOR*, 4%. Furthermore, the individual changes in this pathway were mutually exclusive. Importantly, the SCLC cells harboring active *PIK3CA* mutations were potentially targetable with currently available PI3K inhibitors.

Conclusions: The PI3K/AKT/mTOR pathway is distinguishable in SCLC genomic alterations. Therefore, a sequencing-based comprehensive analysis could stratify SCLC patients by potential therapeutic targets.

Key Words: Lung cancer, Small cell, Genome, Comprehensive, PI3K/AKT/mTOR.

(*J Thorac Oncol.* 2014;9: 1324–1331)

Small cell lung cancer (SCLC) comprises approximately 15% of all lung cancers,[1] and it is an exceptionally aggressive malignancy with a high proliferative index and an unusually strong predilection for early metastasis.[2] Despite extensive basic and clinical research over the past 30 years, little progress has been made[2] in treating this disease.

A better understanding of the genomic changes in SCLC is essential to identify new therapeutic targets. Genomic analyses have revealed genetically altered therapeutic targets in lung adenocarcinoma[3–5] and squamous cell lung carcinoma.[6] However, a systematic genomic analysis of SCLC is difficult because this cancer subtype is rarely treated surgically, resulting in the lack of suitable tumor specimens for comprehensive analysis.

Two reports regarding the comprehensive genomic analysis of SCLC with a relatively small number of samples have been published recently. These reports suggested that transcriptional deregulation (i.e., via *RB1*, *SOX2*, *MYC* family members and chromatin modifiers) might play a role in SCLC biology.[7,8] However, to date, attempts to develop targeted therapies toward these transcriptional deregulations have had limited success.

Activating alterations to oncogenes, such as receptor tyrosine kinases (RTKs) and PI3K/AKT/mTOR pathway proteins,[9–13] are regarded as successful therapeutic targets. We conducted a comprehensive genomic study in over 50 SCLC cases, and we found a higher penetrance of activating alterations of the PI3K/AKT/mTOR pathway that act in a mutually exclusive manner.

*Division of Thoracic Oncology, National Cancer Center Hospital East; †Exploratory Oncology Research and Clinical Trial Center, National Cancer Center; ‡Pathology Division, Research Center for Innovative Oncology, National Cancer Center Hospital East; §Division of Thoracic Surgery, National Cancer Center Hospital East, Kashiwa, Japan; and ‖Division of Genome Biology, National Cancer Center Research Institute, Chuo-ku, Tokyo, Japan.

This work was partly presented at the Annual Meeting of the American Society of Clinical Oncology, May 31–June 4, 2013, Chicago, IL. This study was performed as a research program of the Project for Development of Innovative Research on Cancer Therapeutics (P-Direct), Ministry of Education, Culture, Sports, Science and Technology of Japan, and it was supported by JSPS KAKENHI Grant Number 24300346, 26870876 and National Cancer Center Research and Development Fund (23-A-8, 15).

Disclosures: The authors declare no conflicts of interest.

Address for correspondence: Katsuya Tsuchihara, MD, PhD, Exploratory Oncology Research and Clinical Trial Center, National Cancer Center, 6-5-1 Kashiwanoha, Kashiwa 277-8577, Japan. E-mail: ktsuchih@east.ncc.go.jp

ISSN: 1556-0864/14/0909-1324

PATIENTS AND METHODS

Samples

This study was approved by the Institutional Review Board (IRB) of the National Cancer Center, Japan (IRB number: 2011-201). All data used in this study were obtained from a database at the Division of Thoracic Oncology, National Cancer Center Hospital East, Kashiwa, Japan.

From July 1992 to March 2012, we consecutively collected 1042 SCLC cases at our hospital. Fifty-five of these cases were included in the current study based on the following criteria: a surgical resection or mediastinoscopy was performed; a re-review confirmed a pathological diagnosis of SCLC; the tumor specimens contained a minimum of 70% tumor cells; enough tissue was obtained for a comprehensive analysis; the patient did not receive any neoadjuvant treatment; and the corresponding normal tissue, which was obtained from paraffin-embedded blocks of resected lung tissue that was microscopically free of cancer cells, was also available for analysis. We analyzed the exomes of these 55 samples to assess their mutational burden.

Depending on the tissue size, three to six sections (10 μm thickness) were cut. For the tumors showing a combined SCLC and other histology, only the SCLC compartment was dissected and used for analysis. Total DNA was obtained from formalin- ($n = 43$) or methanol-fixed ($n = 12$) paraffin-embedded tumors and matched normal tissue samples. All patients (100%) were Japanese.

Among these 55 cases, four exome data sets did not meet the sequence quality requirement and were excluded from further analyses. In addition, 48 samples received copy number analysis using single nucleotide polymorphism array data.

Procedures

The detailed experimental procedures are described in the Supplemental Information section (Supplemental Digital Content 1, http://links.lww.com/JTO/A625)

Whole Exon Sequencing and Copy Number Analysis

The Absolutely RNA FFPE kit (modified protocol for DNA extraction, Agilent Technologies, Santa Clara, CA) was used to prepare the DNA. Using 1 μg of dsDNA, quantified by Quant-iT PicoGreen dsDNA Reagent and Kits (Life Technologies, Carlsbad, CA), the exome-sequencing libraries were prepared. All exomes were captured using the SureSelect Human All Exon V4+UTRs Kit (Agilent Technologies) (71 mb). The exome capture libraries were sequenced by HiSeq 2000 (Illumina, San Diego, CA) to generate 100-bp paired-end data.

The Illumina HumanOmniExpress-FFPE BeadChip assay was used to analyze the genotype, DNA copy number, and loss of heterozygosity (LOH) in 48 primary-normal paired samples. All samples, except for 1 ($n = 47$), passed our quality control metrics for sample identity and data quality. A subset of 693,000 high-quality single nucleotide polymorphisms was selected for all analyses (Supplemental Figure 1, Supplemental Digital Content 2, http://links.lww.com/JTO/A626). A gene was considered copy number amplified if the calculated copy number in a sample was more than or equal to 4, and a gene was considered copy loss if the copy number in a sample was 0. Recurrent genomic regions with DNA copy gain and loss were identified using GISTIC, version 2.0.[14,15]

Identification of Significantly Mutated Genes

Significantly mutated genes were identified according to a previously reported protocol.[16] The length of the total coding sequence regions was represented as N (approximately 39.8 mb). When a patient (patient i) harbored a total of m_i single nucleotide variants (SNVs), the probability that the patient harbored SNVs in gene t (length: n) was calculated as follows:

$$P_{t,i} = 1-(1-\mathrm{m_i}/\mathrm{N})^{\mathrm{n}(t)}$$

The sum of $P_{t,i}$ in 51 samples was represented as the expected number of cases with SNVs in gene t:

$$\mathrm{P}_t = \sum_{i=1}^{51}(1-(1-\mathrm{m_i}/\mathrm{N})^{\mathrm{n}(t)})$$

The p values of the observed number were calculated using the binomial probability function with R pbinom.

Cancer Census Genes and Analysis of Hot Spot Mutations

We defined the cancer census genes as follows: 487 genes listed in the Catalogue of Somatic Mutations in Cancer (COSMIC) database (release version 64; http://cancer.sanger.ac.uk/cancergenome/progects/cosmic/) and 13 genes reported by Peifer et al.[7] were considered candidate driver genes. To analyze hot spot mutations, mutation data from the SCLC cases were downloaded from the COSMIC database (release version 64 or 68).

Cell Lines and Assays

The cell lines were cultured in RPMI-1640 supplemented with 10% fetal bovine serum (FBS) or hydrocortisone, insulin, transferrin, estradiol, and selenium (HITES) medium with 5% FBS. Then, 10,000 cells were plated in three replicates into 96-well plates. After 72 hours incubation with inhibitors, cell viability was analyzed with a WST-8 assay and a Cell Counting Kit-8 (Dojindo, Kumamoto, Japan). Western blotting was performed as described in the Supplemental Information section (Supplemental Digital Content 1, http://links.lww.com/JTO/A625).

RESULTS

Patient Characteristics

The characteristics of the available patient exome data ($n = 51$) are summarized in Table 1 and Supplemental Table 3 (Supplemental Digital Content 3, http://links.lww.com/JTO/A627). Fifty patients received surgical resections and one patient received a mediastinoscopy. Forty-two patients were male and nine were female. The median age at the time of surgical resection was 67 years (range, 42–86 years). Of the 51 patients, 50 (98%) had a history of smoking, and the pathological stages were distributed as follows: stage I, 28 patients; stage II, 13

TABLE 1. Patient Characteristics

Characteristic	No. of Patients
Total	51
Gender	
Male/female	42/9
Age, years	
Median (range)	67 (42–86)
Performance status	
0/1/2	35/15/1
Smoking status	
Never/ever	1/50
Pack years	
Median (range)	47 (0–98)
Histology	
Pure SCLC/combined SCLC	40/11
Pathological stage	
I/II/III/IV	28/13/9/1
Vascular invasion	
Absent/present	8/43
Lymphatic invasion	
Absent/present/unknown	31/19/1
Pleural invasion	
Absent/present/unknown	31/19/1
Tumor diameter	
Median (range)	2.5 (1.1–13.0)

patients; stage III, nine patients; and stage IV, one patient. All patients were positive for at least one of the following neuroendocrine markers: CD56, chromogranin A, or synaptophysin.

Somatic Point Mutations

The exome capture, sequencing, and analysis of the 51 SCLC tumor–normal tissue pairs identified 10,640 protein-altering somatic mutations, including 9376 missense, 707 nonsense, and 557 protein-altering insertions and/or deletions (INDEL) (Supplemental Table 4, Supplemental Digital Content 3, http://links.lww.com/JTO/A627). The SCLC tumors had an average of 209 protein-altering SNVs (range, 41–639) per case, with a mean nonsynonymous mutation rate of 6.15 mutations per mega-base (Supplemental Figure 2, Supplemental Digital Content 2, http://links.lww.com/JTO/A626). Significantly mutated genes are determined as Supplemental Table 5 (Supplemental Digital Content 3, http://links.lww.com/JTO/A627). Overall, 414 genes had a p value of less than 0.01 and 1321 genes had a p value of less than 0.05.

A description of the significantly mutated cancer census genes (p value <0.05 in our data set) is provided in Table 2. Notably, *TP53* was the most frequently mutated gene (mutation frequency of 80%, p value of 5.81E–69). The mutation frequencies and p values of cancer census genes were 39% and 6.42E–22, 16% and 0.00019, 10% and 0.0017 for *RB1*, *ROS1*, and *RET*, respectively. Mutations of histone modifiers were also recurrently identified in this study; *CREBBP* was mutated in 6% of the patients, and *EP300* was mutated in 4% of the patients (Fig. 1). Recently reported candidate driver genes were also recurrently identified in the PI3K/AKT/mTOR signaling pathway. Three patients (6%) had mutations in *PIK3CA* (one E545K, two others), and two patients (4%) had mutations in the *PTEN* C2 domain (Supplemental Figure 3, Supplemental Digital Content 2, http://links.lww.com/JTO/A626).

To validate the whole exon sequencing data, we performed Sanger sequencing for the variants including four SNVs of *PIK3CA* and *ROS1* and a deletion of *KIT* in five individual tumor samples. All the variants detected using whole exon sequencing were reproduced using conventional Sanger sequencing (Supplemental Figure 4, Supplemental Digital Content 2, http://links.lww.com/JTO/A626). Furthermore, we designed a custom target-capturing panel containing all the coding exons of 244 genes. Four tumor samples were applied to the target resequencing, and all 41 SNVs or indels in these tumor genomes were reproducibly identified (Supplemental Table 6, Supplemental Digital Content 3, http://links.lww.com/JTO/A627).

Copy Number Analysis

Next, we applied a novel algorithm to identify the significant somatic copy number alterations (Supplemental Figure 5, Supplemental Digital Content 2, http://links.lww.com/JTO/A626). A description of frequently amplified cancer census genes (GISTIC $-\log_{10}$ q score ≥ 1.50) is provided in Table 3. *MYC* family members were frequently amplified (GISTIC q scores were 2.50, 1.65, and 1.57 for *MYCL1*, *MYCN*, and *MYC*, respectively). The amplifications affected *MYCL1* (4/47 cases), *MYC* (1/47 cases), and *MYCN* (1/47 cases). All *MYC* family member amplifications (13% of cases) were mutually exclusive (Fig. 1). In addition, gene amplifications were frequently found in the PI3K/AKT/mTOR signaling pathway (GISTIC q scores were 2.45 and 1.22 for *AKT2* and *RICTOR*, respectively). The gene amplifications in PI3K/AKT/mTOR signaling were observed in *AKT2* (4/47 cases) and *RICTOR* (3/47 cases), and they were also mutually exclusive (Fig. 1). Previously reported amplifications involving *SOX2* (1/47 cases) and *KIT* (1/47 cases) were also identified.

Recurrent Mutations at the Same Position

Forty genes with recurrent somatic mutations at the same position were identified in this study and the COSMIC database (Table 4). *TP53*, the well-characterized tumor suppressor gene, had 29 different positions that mutated more than or equal to two times (total recurrent samples, 134). *RB1* had four different positions that mutated two or three times. The remaining 38 genes had one position that mutated two or three times. Well-established activating mutations in *PIK3CA*, the catalytic subunit of phosphoinositide-3 kinase (E545), were also detected in another SCLC cohort.

PI3K/AKT/mTOR Pathway Alteration

Because of the large number of somatic point mutations and focal amplifications found in the PI3K/AKT/mTOR signaling pathway (e.g., *PIK3CA*, *PTEN*, *AKT2*, and *RICTOR*), we focused our investigation on the changes in the PI3K/AKT/mTOR pathway. We observed that the PI3K/AKT/mTOR pathway was altered in 17/47 (36%) of the SCLC tumors (Fig. 1), and all altered genes in the PI3K/AKT/mTOR pathway were mutually exclusive. There was no difference in the

TABLE 2. Significantly Mutated Cancer Census Genes (*$p < 0.05$ in This Study)

	This Data Set ($n = 51$)			COSMIC Database	
Symbol	Mutated Case	Mutation Frequency (%)	p Value*	Mutated Case/Total	Mutation Frequency (%)
TP53	41	80	5.81E–69	235/308	76
RB1	20	39	6.42E–22	99/181	55
ROS1	8	16	0.00019	7/65	11
RET	5	10	0.0017	4/147	3
IKZF1	4	8	0.0017	0/57	0
CD79B	2	4	0.0042	0/61	0
PAX7	3	6	0.0074	3/63	5
HIP1	4	8	0.0076	1/62	2
CDH11	4	8	0.0086	0/62	0
MN1	4	8	0.014	1/61	2
PTEN	2	4	0.017	39/309	13
ERBB2	4	8	0.018	1/167	1
LPP	3	6	0.019	0/62	0
MLL2	6	12	0.021	7/57	12
BCL11B	3	6	0.022	0/63	0
LMO1	1	2	0.023	0/62	0
NR4A3	3	6	0.028	1/56	2
ZNF521	4	8	0.031	10/62	16
PIK3CA	3	6	0.034	38/272	14
WT1	2	4	0.040	1/127	1
TRIM33	3	6	0.041	1/62	2
PBRM1	4	8	0.042	1/61	2
FUS	2	4	0.043	0/62	0
ABL1	3	6	0.044	2/63	3
RPN1	2	4	0.045	0/57	0
BTG1	1	2	0.045	0/62	0

*p value., P binom.

clinical characteristics, such as smoking status, gender, and age, between the PI3K/AKT/mTOR pathway-affected group (Group A) and the PI3K/AKT/mTOR pathway-unaffected group (Group B). The frequencies of *TP53* and *RB1* mutations were identical between Group A and Group B. However, more *MYC* family genes tended to be amplified in Group B; Group A did not harbor *KRAS* or *BRAF* mutations, and most patients in Group A did not have MAPK/ERK pathway changes.

The correlation between the PI3K/AKT/mTOR pathway changes and RTKs is shown in Supplemental Figure 6 (Supplemental Digital Content 2, http://links.lww.com/JTO/A626). The changes in various targetable RTK genes were detected, such as *ERBB2* ($n = 4$), *KIT* ($n = 2$), *PDGFRA* ($n = 3$), *PDGFRB* ($n = 2$), *KDR* ($n = 3$), *MET* ($n = 1$), *ROS1* ($n = 8$), and *RET* ($n = 5$). However, none of these genes showed a recurrent mutation at the same point in this data set or the COSMIC database. The PI3K/AKT/mTOR pathway status did not correlate with the RTK changes.

Drug Sensitivity

To further investigate whether the PI3K/AKT/mTOR pathway could be a feasible therapeutic target in SCLC, we tested the in vitro drug sensitivity of the SCLC cell lines using the clinically developed compounds targeting this pathway (Fig. 2 and Supplemental Figure 7, Supplemental Digital Content 2, http://links.lww.com/JTO/A626). We selected three SCLC cell lines with genetic alterations in the PI3K/AKT/mTOR pathway: H446 (*PTEN*-loss, *MYC*-amplified), H1048 (*PIK3CA* mutation), and H1694 (*AKT3*-amplified). We also examined H82 (*MYC*-amplified) and H209, which do not display activation of the PI3K/AKT/mTOR pathway. Using these cell lines, we assessed the efficacy of four compounds that inhibit the PI3K/AKT/mTOR pathway and are in on-going phase I/II trials: BEZ235 (PI3K and mTOR inhibitor), BKM120 (PI3K inhibitor), INK128 (mTOR inhibitor), and MK2206 (AKT inhibitor), as well as one cytotoxic agent, cisplatin. None of the cell lines showed apparent cytotoxicity in response to doses up to 1 μM cisplatin. Conversely, all PI3K/AKT/mTOR inhibitors significantly impaired the proliferation of the SCLC cell lines. H1048, which harbors a *PIK3CA* mutation (H1047R), was the most sensitive to all of the PI3K/AKT/mTOR inhibitors, with IC50 values of 3.8, 5.4, 99.9, and 195.4 nM for INK128, BEZ235, MK2206, and BKM120, respectively. BEZ235 was the most effective compound to specifically inhibit H1048 cell growth

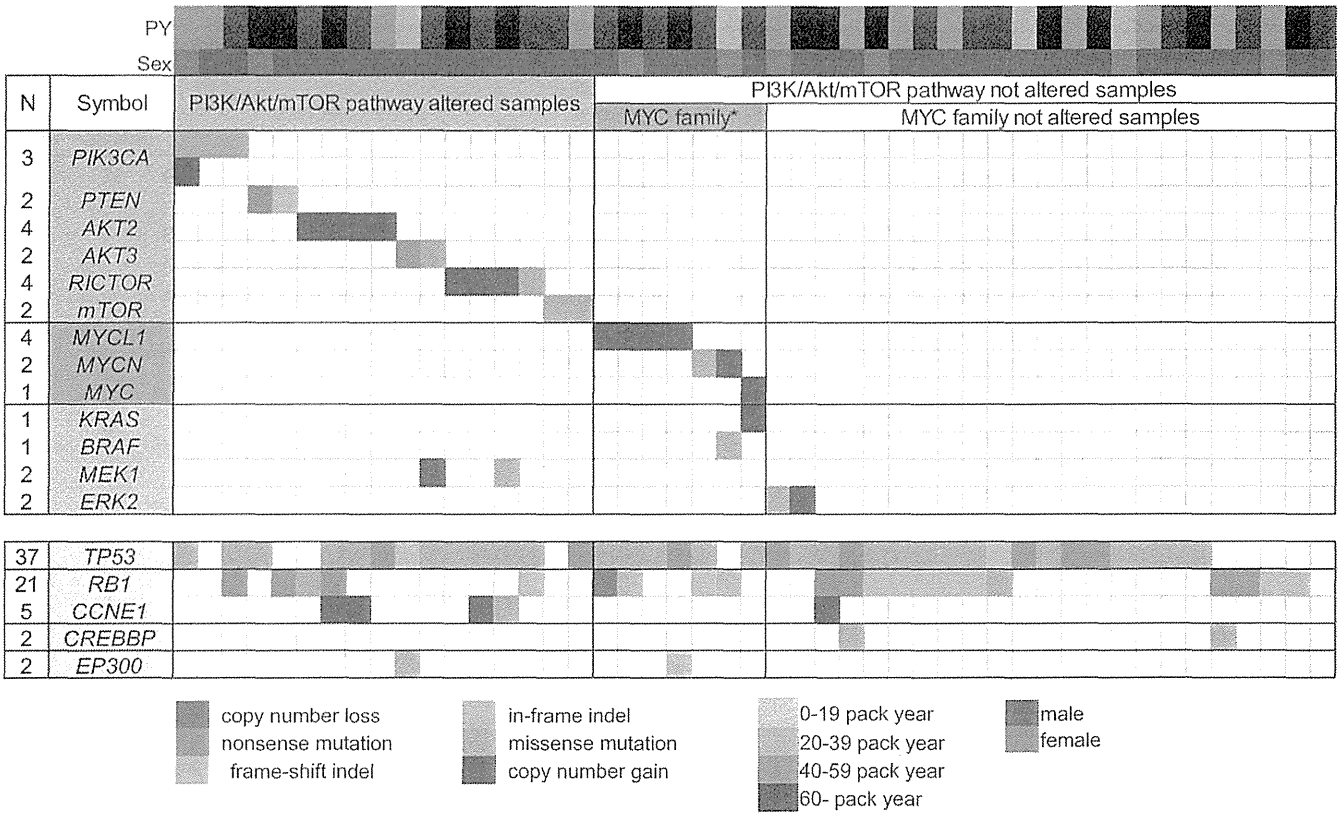

FIGURE 1. An overview of the key driver mutations and major associated clinical features of 47 SCLC samples. The number of events per gene is noted on the left. The genes are displayed as rows, and the samples are displayed as columns, with major associated clinical features.
PY, PACK YEARS; MYC FAMILY*, MYC FAMILY ALTERED SAMPLES.

TABLE 3. Frequently Mutated Cancer Census Genes ($-\log_{10}$ *q* score ≥1.5)

	This Data Set ($n = 47$)
Symbol	**$-\log_{10}$ (q score)**
MYB	3.40
MYCL1	2.50
AKT2	2.45
CLTCL1	2.34
LIFR	2.21
IL7R	2.13
THRAP3	2.09
ETV5	2.05
BCL6	1.99
EIF4A2	1.93
LPP	1.89
PAX5	1.89
ZNF384	1.86
ARID1A	1.65
MYCN	1.65
FANCG	1.65
MYC	1.57
MDS2	1.52

(IC50 = 5.4), with an IC50 value greater than 10-fold lower than that of H82 (IC50 = 58.3 nM) and fivefold lower than that of H209 (IC50 = 29.7 nM). In contrast, H446 (IC50 = 33.3 nM) and H1694 cells (IC50 = 52.5 nM) were relatively resistant to BEZ235 treatment.

The impact of BEZ235 on AKT phosphorylation in SCLC cells was investigated using Western blot analysis. AKT was activated in the H446 and H1048 cells under these culture conditions, and it was effectively inhibited after being treated with 10 nM BEZ235. Conversely, constitutive phosphorylation of AKT was not observed in H1694 cells, even when pan-AKT was over-expressed. In addition, AKT phosphorylation was not detected in the H82 and H209 cells. Regarding factors located downstream of mTOR, S6RP was phosphorylated in all five SCLC cell lines. Especially, the phosphorylation level was high in AKT-activated H446 and H1048 cells. BEZ235 significantly reduced the phosphorylation of S6RP in all the cells.

To evaluate the contribution of PI3K/AKT/mTOR signaling to SCLC cell proliferation, we used RNA interference (RNAi) to down-regulate the expression of *PIK3CA* in H1048 cells. The transient silencing of *PIK3CA* impaired the phosphorylation of AKT and S6RP (Supplemental Figure 8, Supplemental Digital Content 2, http://links.lww.com/JTO/A626). In addition, *PIK3CA* silencing induced a decrease in the proliferation of H1048 cells.

TABLE 4. The Recurrent Mutations Detected at the Same Position in This Study and the COSMIC Database

Gene	Recurrent in This Study (no.)	No. in This Data Set	Recurrent in COSMIC Database (no.)	No. in COSMIC Database	Total
TP53	Q38 (1) T155 (1) V157 (1) R158 (2) A159 (1) M160 (1) A161 (1) Y163 (2) R175 (1) C176 (2) H179 (1) Q192 (1) D208 (1) R209 (1) R213 (1) S215 (2) Y220 (1) R248 (1) R249 (2) L265 (1) G266 (2) R273 (1) R283 (2) E286 (1) E294 (1) E298 (1) Q317 (1) R337 (2) R342 (1)	37	Q38 (1) T155 (4) V157 (11) R158 (3) A159 (1) M160 (1) A161 (1) Y163 (2) R175 (4) C176 (2) H179 (7) Q192 (2) D208 (1) R209 (2) R213 (3) S215 (1) Y220 (8) R248 (7) R249 (11) L265 (1) G266 (3) R273 (8) R283 (1) E286 (5) E294 (3) E298 (2) Q317 (1) R342 (1)	97	134
RB1	T543 (2) W78 (1) W195 (1) E322 (1)	5	W78 (1) W195 (2) E322 (1)	4	9
ABRA	S276 (2)	2		0	2
AP3M2	T72 (2)	2		0	2
CLEC4G	R23 (2)	2		0	2
DACT1	V481 (2)	2		0	2
DPP6	Q345 (2)	2		0	2
DUSP27	D886 (2)	2		0	2
GPR149	R540 (2)	2		0	2
KIAA2022	Q738 (2)	2		0	2
OR9G1	C168 (2)	2		0	2
PCDHGA5	E782 (2)	2		0	2
PDE4C	P39 (2)	2		0	2
PJA1	E182 (2)	2		0	2
ZFP1	Q287 (2)	2		0	2
B2M	M1 (1)	1	M1 (2)	2	3
PIK3CA	E545 (1)	1	E545 (2)	2	3
AFF2	D506 (1)	1	D506 (1)	1	2
ASTN1	R184 (1)	1	R184 (1)	1	2
BEND3	G263 (1)	1	G263 (1)	1	2
C8A	R438 (1)	1	R438 (1)	1	2
CREB3L3	P82 (1)	1	P82 (1)	1	2
CST4	R46 (1)	1	R46 (1)	1	2
DEFB112	R112 (1)	1	R112 (1)	1	2
GPR139	T322 (1)	1	T322 (1)	1	2
HCN1	Q772 (1)	1	Q772 (1)	1	2
ITGA4	R481 (1)	1	R481 (1)	1	2
JAM3	Y31 (1)	1	Y31 (1)	1	2
KCNJ12	R261 (1)	1	R261 (1)	1	2
LIFR	Q978 (1)	1	Q978 (1)	1	2
LRRC52	A258 (1)	1	A258 (1)	1	2
MED23	N1095 (1)	1	N1095 (1)	1	2
MUC6	P27 (1)	1	P27 (1)	1	2
OPN4	C303 (1)	1	C303 (1)	1	2
OR10S1	A283 (1)	1	A283 (1)	1	2
OR2W1	I206 (1)	1	I206 (1)	1	2
OR5F1	S265 (1)	1	S265 (1)	1	2
OR5L1	S267 (1)	1	S267 (1)	1	2
SLC28A3	Q261 (1)	1	Q261 (1)	1	2
ZNF382	C278 (1)	1	C278 (1)	1	2

no., number Recurrent (no.), positions with recurrent mutations (no. of instances).

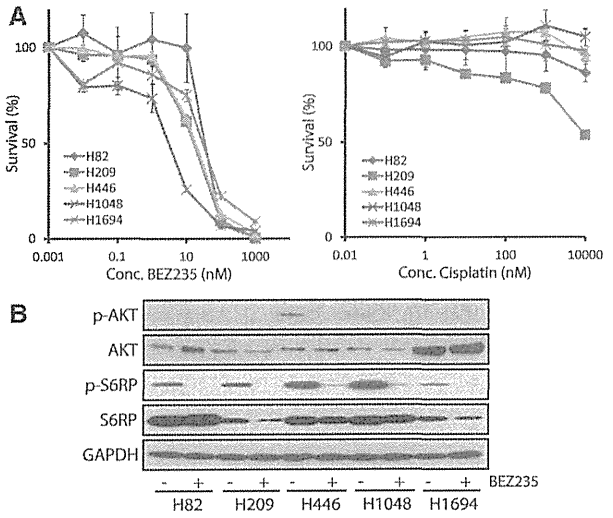

FIGURE 2. (*A*) The concentration–response cell survival curves of SCLC cell lines with or without genetic alteration in the PI3K/AKT/mTOR pathway in response to BEZ235 (nM) and Cisplatin (nM). The *PIK3CA* mutation positive cell line, H1048, is relatively sensitive to BEZ235. The H82 and H209 cell lines are negative controls. (*B*) Western blotting was used to investigate the impact of BEZ235 on AKT phosphorylation and S6RP phosphorylation in the SCLC cells. AKT was activated in H446 and H1048 cells, and it was inhibited after being treated with 10 nM BEZ235. AKT was amplified but not constitutively phosphorylated in the H1694 cells. AKT phosphorylation was not detected in the negative control cell lines, H82 and H209. With regard to factors located downstream of mTOR, S6RP was phosphorylated in all five SCLC cell lines. Especially, the phosphorylation level was high in AKT-activated H446 and H1048 cells. BEZ235 significantly reduced the phosphorylation of S6RP in all the cells.

DISCUSSION

We performed an integrative genomic analysis of SCLC in Japanese patients. The SCLC tumors had a significantly high mutation rate. An analysis of the base-level transitions and transversions showed that G-to-T transversions were predominant (Supplemental Figure 2, Supplemental Digital Content 2, http://links.lww.com/JTO/A626), which was consistent with the demonstrated effects of tobacco smoke carcinogens on DNA.[8,17] A high prevalence of inactivating mutations in *TP53* and *RB1* and recently reported candidate driver genes, including the mutations of histone modifiers (*CREBBP*[7] and *EP300*[7]), were recurrently observed along with the amplification of *MYC* family members.[7,14,18,19] These data indicate that the genomic landscape of SCLC is equivalent between Asian and Caucasian populations.[7,8,17,18]

SCLC is characterized by aggressive growth and a poor prognosis, and no single molecular targeted drug has shown any clinical efficacy over an extended period. A number of inhibitors targeting changes in RTKs are currently used in clinical use. Alterations in well-known, targetable RTK genes, such as *ERBB2*, *KIT*, *PDGFRA*, *PDGFRB*, *KDR*, *MET*, *ROS1*, and *RET*, were detected in this study. However, these alterations did not overlap with previously reported activating mutations.

The PI3K/AKT/mTOR signaling pathway is involved in the survival, proliferation, and migration of SCLC cell lines.[13] We confirmed the activation of the PI3K pathway in the SCLC-derived cell lines. AKT protein overexpression was observed in the *AKT3*-amplified H1694 cells, and phosphorylated-AKT and S6RP were increased in the *PTEN*-lacking H446 cells and *PIK3CA*-mutated H1048 cells. In addition, the significant decrease in the proliferation of H1048 cells induced by *PIK3CA* silencing suggested that the proliferation of these cells was strongly dependent on the PI3K/AKT/mTOR pathway (Supplemental Figure 8, Supplemental Digital Content 2, http://links.lww.com/JTO/A626). Consistently, genetic changes in the PI3K/AKT/mTOR pathway were detected in approximately 40% of our clinical samples. In addition to high penetrance, these alterations occurred in a mutually exclusive manner. A similar trend was observed in another Japanese cohort of primary SCLC (Supplemental Table 7, Supplemental Digital Content 3, http://links.lww.com/JTO/A627). In addition to SCLC, a significant exclusion pattern among PI3K pathway molecules was observed in the systematic analysis of breast cancer genomes.[20] Together, these data suggest indispensable roles for this pathway in tumorigenesis.

Two specific inhibitors of mTORC1, everolimus[10] and temsirolimus,[11] were tested against SCLC in a Phase II study. However, single-agent antitumor activity was limited in unselected patients; the response rate in these studies was less than 10%. To improve the response to these inhibitors, the addition of PI3K inhibition has been suggested. The dual inhibition of PI3K and mTOR might be advantageous over single inhibition by suppressing a S6K feedback loop that leads to the pathway reactivation.[21] Based on this idea, an on-going phase I study of the PI3K and mTORC1/2 dual inhibitor, BEZ235, was designed for the patients with advanced solid tumors harboring *PIK3CA* or *PTEN* alteration (NCT01195376). In this study, we showed that the survival of the cisplatin-resistant SCLC cell lines was well suppressed by BEZ235, accompanied by the suppression of S6RP phosphorylation. Notably, the effect was most significant against H1048 cells, which harbor a *PIK3CA*-activating mutation.

However, we found that not all SCLC cell lines harboring PI3K/AKT/mTOR pathway alterations exhibited a similar sensitivity to BEZ235. Although AKT phosphorylation was significantly inhibited by BEZ235 in both the H446 cells and H1048 cells, the sensitivity of the H446 cells was less than that of the H1048 cells. *MYC* gene amplification reportedly evades PI3K-targeted therapy.[22] *MYC* amplification was demonstrated in H446 cells,[23,24] and this co-alteration could be one cause of the observed low sensitivity. Thus, to determine the most beneficial concentrations for patients, both direct target molecules and other interfering signaling pathways should be simultaneously assessed. In this study, no surgically resected tumors harbored co-alterations of the PI3K/AKT/mTOR pathway and MYC gene amplification. However, the sample size of this study and other published systemic analyses remained small, and many of the samples were obtained from relatively early-stage tumors. We should expand the sample size and further analyze samples of advanced tumors using biopsy, necropsy, and autopsy specimens to clarify the coexistence of oncogenic alterations in SCLC.

Although further large-scale validation studies are needed, our data suggest that evaluating the genetic status of molecules that modify the PI3K/AKT/mTOR signaling pathway, such as MYC family and MAPK pathway molecules, is essential to select patients with potential sensitivity to PI3K/AKT/mTOR inhibitors. In other words, enriching the study population by performing the integrative genomic analysis is essential when performing phase studies of PI3K/AKT/mTOR inhibitors in SCLC.

In conclusion, the SCLC genome possesses distinguishable genetic features in the PI3K/AKT/mTOR pathway. Genetic alterations in the PI3K/AKT/mTOR pathway were noted as a top therapeutic priority in SCLC. In addition to surgically resected samples, advanced tumors should be examined for comprehensive genomic analysis.

ACKNOWLEDGMENTS

This study was performed as a research program of the Project for Development of Innovative Research on Cancer Therapeutics (P-Direct), Ministry of Education, Culture, Sports, Science and Technology of Japan, and it was supported by JSPS KAKENHI Grant Number 24300346 and National Cancer Center Research and Development Fund (23-A-8, 15). The authors thank Ms. Fumiko Koh, Drs. Masao Yamaguchi, Hideki Okada, Keiju Aokage, Tomoyuki Hishida, Junji Yoshida, Keisuke Kirita, Eri Sugiyama, Yoshitaka Zenke, Tatsuya Yoshida, Yuji Matsumoto, and Yuuki Matsumura for their support and comments.

REFERENCES

1. Siegel R, Naishadham D, Jemal A. Cancer statistics, 2012. *CA Cancer J Clin* 2012;62:10–29.
2. William WN Jr, Glisson BS. Novel strategies for the treatment of small-cell lung carcinoma. *Nat Rev Clin Oncol* 2011;8:611–619.
3. Govindan R, Ding L, Griffith M, et al. Genomic landscape of non-small cell lung cancer in smokers and never-smokers. *Cell* 2012;150:1121–1134.
4. Kohno T, Ichikawa H, Totoki Y, et al. KIF5B-RET fusions in lung adenocarcinoma. *Nat Med* 2012;18:375–377.
5. Lipson D, Capelletti M, Yelensky R, et al. Identification of new ALK and RET gene fusions from colorectal and lung cancer biopsies. *Nat Med* 2012;18:382–384.
6. Cancer Genome Atlas Research Network. Comprehensive genomic characterisation of squamous cell lung cancers. *Nature* 2012; 489: 519–525.
7. Peifer M, Fernández-Cuesta L, Sos ML, et al. Integrative genome analyses identify key somatic driver mutations of small-cell lung cancer. *Nat Genet* 2012;44:1104–1110.
8. Rudin CM, Durinck S, Stawiski EW, et al. Comprehensive genomic analysis identifies SOX2 as a frequently amplified gene in small-cell lung cancer. *Nat Genet* 2012;44:1111–1116.
9. Pietanza MC, Ladanyi M. Bringing the genomic landscape of small-cell lung cancer into focus. *Nat Genet* 2012;44:1074–1075.
10. Tarhini A, Kotsakis A, Gooding W, et al. Phase II study of everolimus (RAD001) in previously treated small cell lung cancer. *Clin Cancer Res* 2010;16:5900–5907.
11. Pandya KJ, Dahlberg S, Hidalgo M, et al. A randomised, phase II trial of two dose levels of temsirolimus (CCI-779) in patients with extensive-stage small-cell lung cancer who have responding or stable disease after induction chemotherapy: a trial of the Eastern Cooperative Oncology Group (E1500). *J Thorac Oncol* 2007;2:1036–1041.
12. Voortman J, Lee JH, Killian JK, et al. Array comparative genomic hybridization-based characterization of genetic alterations in pulmonary neuroendocrine tumors. *Proc Natl Acad Sci U S A* 2010;107: 13040–13045.
13. Wojtalla A, Fischer B, Kotelevets N, et al. Targeting the phosphoinositide 3-kinase p110-α isoform impairs cell proliferation, survival, and tumor growth in small cell lung cancer. *Clin Cancer Res* 2013;19:96–105.
14. Mermel CH, Schumacher SE, Hill B, Meyerson ML, Beroukhim R, Getz G. GISTIC2.0 facilitates sensitive and confident localization of the targets of focal somatic copy-number alteration in human cancers. *Genome Biol* 2011;12:R41.
15. Beroukhim R, Getz G, Nghiemphu L, et al. Assessing the significance of chromosomal aberrations in cancer: methodology and application to glioma. *Proc Natl Acad Sci U S A* 2007;104:20007–20012.
16. Suzuki A, Mimaki S, Yamane Y, et al. Identification and characterization of cancer mutations in Japanese lung adenocarcinoma without sequencing of normal tissue counterparts. *PLoS One* 2013;8:e73484.
17. Pleasance ED, Stephens PJ, O'Meara S, et al. A small-cell lung cancer genome with complex signatures of tobacco exposure. *Nature* 2010;463:184–190.
18. Arriola E, Cañadas I, Arumí M, Rojo F, Rovira A, Albanell J. Genetic changes in small cell lung carcinoma. *Clin Transl Oncol* 2008;10:189–197.
19. Iwakawa R, Takenaka M, Kohno T, et al. Genome-wide identification of genes with amplification and/or fusion in small cell lung cancer. *Genes Chromosomes Cancer* 2013;52:802–816.
20. Cancer Genome Atlas Network. Comprehensive molecular portraits of human breast tumours. *Nature* 2012; 490: 61–70.
21. Gadgeel SM, Wozniak A. Preclinical rationale for PI3K/Akt/mTOR pathway inhibitors as therapy for epidermal growth factor receptor inhibitor-resistant non-small-cell lung cancer. *Clin Lung Cancer* 2013;14:322–332.
22. Ilic N, Utermark T, Widlund HR, Roberts TM. PI3K-targeted therapy can be evaded by gene amplification along the MYC-eukaryotic translation initiation factor 4E (eIF4E) axis. *Proc Natl Acad Sci U S A* 2011;108:E699–E708.
23. Brennan J, O'Connor T, Makuch RW, et al. myc family DNA amplification in 107 tumors and tumor cell lines from patients with small cell lung cancer treated with different combination chemotherapy regimens. *Cancer Res* 1991;51:1708–1712.
24. Sos ML, Dietlein F, Peifer M, et al. A framework for identification of actionable cancer genome dependencies in small cell lung cancer. *Proc Natl Acad Sci U S A* 2012;109:17034–17039.

European Journal of Radiology 83 (2014) e23–e35

Contents lists available at ScienceDirect

European Journal of Radiology

journal homepage: www.elsevier.com/locate/ejrad

Review

Primary staging of laryngeal and hypopharyngeal cancer: CT, MR imaging and dual-energy CT

Hirofumi Kuno[a,*], Hiroaki Onaya[b,1], Satoshi Fujii[c,2], Hiroya Ojiri[d,3], Katharina Otani[e,4], Mitsuo Satake[a,5]

[a] Diagnostic Radiology Division, National Cancer Center Hospital East, 6-5-1, Kashiwanoha, Kashiwa, Chiba 277-8577, Japan
[b] Diagnostic Radiology Division, National Cancer Center Hospital, 5-1-1 Tsukiji Chuo-ku, Tokyo 104-0045, Japan
[c] Pathology Division, Research Center for Innovative Oncology, National Cancer Center Hospital East, 6-5-1 Kashiwanoha, Kashiwa, Chiba 277-8577, Japan
[d] Department of Radiology, Jikei University School of Medicine, 3-25-18 Nishi-shinbashi Minato-ku, Tokyo 105-8461, Japan
[e] Imaging & Therapy Systems Division, Siemens Japan K.K., Gate City Osaki West Tower 1-11-1 Osaki, Shinagawa-ku, Tokyo 141-8644, Japan

ARTICLE INFO

Article history:
Received 12 April 2013
Received in revised form 23 July 2013
Accepted 20 October 2013

Keywords:
Laryngeal cancer
Hypopharyngeal cancer
Computed tomography
Magnetic resonance imaging
Dual-energy CT
Staging

ABSTRACT

Laryngeal and hypopharyngeal cancer, in particular T4a disease associated with cartilage invasion and extralaryngeal spread, needs to be evaluated accurately because treatment can impact heavily on a patient's quality of life. Reliable imaging tools are therefore indispensible. CT offers high spatial and temporal resolution and remains the preferred imaging modality. Although cartilage invasion can be diagnosed with acceptable accuracy by applying defined criteria for combinations of erosion, lysis and transmural extralaryngeal spread, iodine-enhanced tumors and non-ossified cartilage are sometimes difficult to distinguish. MR offers high contrast resolution for images without motion artifacts, although inflammatory changes in cartilage sometimes resemble cartilage invasion. With dual-energy CT, combined iodine overlay images and weighted average images can be used for evaluation of cartilage invasion, since iodine enhancement is evident in tumor tissue but not in cartilage. Extralaryngeal spread can be evaluated from CT, MR or dual-energy CT images and the routes of tumor spread into the extralaryngeal soft tissue must be considered; (1) via the thyrohyoid membrane along the superior laryngeal neurovascular bundle, (2) via the inferior pharyngeal constrictor muscle, and (3) via the cricothyroid membrane. Radiologists need to understand the advantages and limitations of each imaging modality for staging of laryngeal and hypopharyngeal cancer.

1. Introduction

Laryngeal and hypopharyngeal cancers are common malignant tumors in the head and neck, and most of such cases are squamous cell carcinomas [1]. In view of the functional and social importance of the larynx, any decision about the optimal management strategy for laryngeal or hypopharyngeal cancer must involve consideration of both potential survival and the functional consequences of any given treatment approach. Patients with T1, T2 and limited cartilage invasion disease can be considered positively for organ-preserving procedures such as radiation therapy alone, a combination of chemotherapy and radiation therapy, and function-preserving partial laryngectomy procedures [2–6]. Patients with T4a disease, particularly when the tumor extends through the cartilage into the soft tissue of the neck, often need aggressive treatments such as total laryngectomy [2,7,8], because the risks of recurrence and cartilage necrosis after radiotherapy alone are high [2–4]. Both CT and MR imaging are routinely used to differentiate between limited and gross cartilage invasion. However, cartilage invasion is sometimes overestimated, resulting in unnecessary total laryngectomies in some patients [9,10].

Currently, dual-energy CT is being investigated in several clinical fields [11–15], including the evaluation of head and neck cancer [16]. Since treatment is decided according to the precise extent and invasion pattern of a tumor, the findings of these imaging procedures play a crucial role in any multidisciplinary approach for management of laryngeal and hypopharyngeal cancer [17–19]. Rapid technological developments in recent years have made it necessary for all members of multidisciplinary teams to understand the

* Corresponding author. Tel.: +81 4 7133 1111x91311; fax: +81 4 7131 4724.
E-mail addresses: hkuno@east.ncc.go.jp (H. Kuno), honaya@ncc.go.jp (H. Onaya), sfujii@east.ncc.go.jp (S. Fujii), ojiri@jikei.ac.jp (H. Ojiri), katharina.otani@siemens.com (K. Otani), msatake@east.ncc.go.jp (M. Satake).
[1] Tel.: +81 3 3542 2511.
[2] Tel.: +81 4 7133 1111.
[3] Tel.: +81 3 3433 1111.
[4] Tel.: +81 3 3493 7429.
[5] Tel.: +81 4 7133 1111.

0720-048X/$ – see front matter © 2013 Elsevier Ireland Ltd. All rights reserved.
http://dx.doi.org/10.1016/j.ejrad.2013.10.022

Table 1
Primary tumor (T) staging according to the American Joint Committee on Cancer (AJCC) 7th edition (modified version by author).

	Laryngeal cancer			Hypopharyngeal cancer
	Supraglottic	Glottic	Subglottic	
T1	One subsite	(a) One vocal cord (b) both vocal cords	Limited to subglottis	≤2 cm and limited to one subsite
T2	More than one subsite	Extends to supra/sub glottis Impaired vocal cord mobility	Extends to glottis	>2–4 cm or more than one subsite
T3	PGS/PES or vocal cord fixation Inner cortex of thyroid cartilage Extends to postcricoid	PGS or vocal cord fixation Inner cortex of thyroid cartilage	Vocal cord fixation	>4 cm or vocal cord fixation
T4a	Tumor invades through the thyroid cartilage or extra-laryngeal spread		Tumor invades thyroid/cricoid cartilage or extra-laryngeal spread	
T4b	Tumor invades prevertebral space, encases carotid artery, or invades mediastinal structures			

Note: PGS = paraglottic space; PES = preepiglottic space.

potential applications, limitations, and appropriate criteria of these imaging modalities.

In this article, we review the significant role of imaging for staging of laryngeal and hypopharyngeal cancer. We discuss the appearances of T4a disease on conventional CT and MR images and illustrate how dual-energy CT can be applied for evaluation of laryngeal and hypopharyngeal cancer.

2. Primary tumor staging (T) of laryngeal and hypopharyngeal cancer

The system for staging of primary laryngeal (glottic, supraglottic and subglottic) and hypopharyngeal cancer is outlined in Table 1 (American Joint Committee on Cancer 2010) [20]. Clinical staging of the primary site is based on involvement of various subsites of the larynx or adjacent regions of the pharynx and vocal cord mobility. Assessment of the primary tumor is initially accomplished by clinical inspection, using indirect mirror and direct endoscopic examination with a fiberoptic nasolaryngoscope. However, these tumors have a tendency to spread submucosally, and this extension into deeply seated tissue planes can be easily missed by clinical examination alone [8,17,19]. Therefore, clinicians rely on imaging to predict which patients will have T3–4 disease. Even if the primary tumor has been clinically diagnosed as T1–2 disease on the basis of inspection, imaging is an important adjunct to exclude any T3–4 factor features or the presence of submucosal extension [8,21–23]. Therefore, cross-sectional imaging using CT or MR imaging is mandatory for completing the staging process, and should be included in the diagnostic workup.

For laryngeal cancer, the first imaging criterion that defines T3 lesions is extension into the paraglottic and/or preepiglottic space, irrespective of vocal cord mobility. In addition, tumor erosion limited to the inner cortex of the thyroid cartilage indicates a T3 lesion, whereas erosion of the outer cortex of the thyroid cartilage define a T4a tumor. For hypopharyngeal cancer, unlike the larynx, criteria that define T3 lesions are based on vocal cord mobility and tumor diameter only. Hypopharyngeal cancer with invasion of the thyroid or cricoid cartilage indicates a T4a lesion, even in cases of localized cartilage invasion. In any event, accurate staging requires diagnosis of subtle cartilage invasion.

Extralaryngeal tumor spread is also one of the important predictors of T4a disease, with or without cartilage invasion, in laryngeal and hypopharyngeal cancer.

3. Technical considerations for CT, MR imaging and dual-energy CT

3.1. Conventional CT

CT is the preferred imaging method for staging of laryngeal and hypopharyngeal cancer. The images are obtained with the patient supine and during quiet respiration (not while holding the breath). The neck should be in slight extension, and the head is aligned along the cephalocaudal axis to allow comparison of symmetrical structures. Malpositioning may create an appearance that simulates disease. Every effort should be made to make the patient feel comfortable. When a small tumor is suspected, the patient may be scanned during a modified Vasalva maneuver or during phonation to open the piriform sinuses [24,25]. Typically, a 100-mL injection of 300 mgI/mL iodinated contrast medium is injected at a rate of 2.5 mL/s and the scan is initiated 70 s after the start of the injection, proceeding in a cranio-caudal direction. The scan range is set from the base of the skull to the bottom of the neck. Reconstructed images are generated as frontal and coronal sections parallel and vertical to the vocal cords from 1 cm above the hyoid bone to the inferior margin of the cricoid cartilage (2-mm thickness and 16-cm field of view).

3.2. MR imaging

MR imaging is also obtained with the patient supine and during quiet respiration. Axial T2-weighted fast spin echo (FSE) and T1-weighted FSE images are obtained with a scan orientation parallel to the true vocal cords. Typical image parameters for a standard examination include a slice thickness of 3 mm with a 1-mm intersection gap. Additional axial fat-saturated T1-weighted fast field echo (FFE) images after intravenous administration of gadolinium chelates are obtained routinely. When evaluations using CT alone are insufficient to determine cartilage invasion, the following 3D sequences are additionally performed within the area from 1 cm above the hyoid bone to the inferior margin of the cricoid cartilage: a 3D-T2-weighted image (3D-T2WI) is acquired in the transverse plane with a 3D volume isotropic T2-weighted acquisition (VISTA) sequence (TR/TE, 1,100/91 with Driven Equilibrium [DRIVE] technique; flip angle, 90; field of view, 230 mm; matrix, 190 × 448; slice thickness/gap, 1.5 mm/0 mm). A 3D-T1-weighted image (3D-T1WI) is then acquired in the transverse plane with a 3D Turbo Field Echo (TFE) sequence unenhanced (TR/TE, 6/2.3; flip angle,